

DESIGN AND VALIDATION OF A FORCED MOTION VARIABLE STIFFNESS AEROELASTIC WIND TUNNEL APPARATUS (AATB)

J. Ertveldt*, **J. Schoukens****, **R. Pintelon****, **S. Vanlanduit***
Vrije Universiteit Brussel: * Department MECH, ** Department ELEC

Keywords: *Unsteady aerodynamics, forced motion, pitch and plunge, aeroelasticity, wind tunnel*

Abstract

The Active Aeroelastic Test Bench (AATB) is designed for the study of low subsonic unsteady aerodynamics and aeroelasticity. The AATB is equipped with four linear motors offering separate control of the pitch and plunge position of the wing. The AATB allows to perform forced motion unsteady aerodynamic experiments when operated in open loop. In addition, when operated in closed loop, aeroelastic experiments can be performed, with both linear, or nonlinear variable structural behaviour.

For this closed-loop operation the directly measured loads are fed back to the real-time controller. This controller then outputs the user desired position, emulating structural behaviour of the wing.

1 Introduction

In the progressive attempt to further reduce aircraft mass, the accurate modelling of aircraft flight dynamics and aeroelastic behaviour becomes more and more important [1]. One of the issues with flexible and light aircraft are, for example, the increased gust response and the increased alteration of manoeuvrability through the larger deformations of the airframe. For that reason, gust load alleviation through passive or active design, is an important research topic these days [2, 3]. These methods, however, have to rely on an accurate model, which takes into account the flexibility of the aircraft.

Different numerical methods exist to build low and high-fidelity flexible aircraft models for the analysis of flight characteristics, and the design of the load alleviation systems [2–4]. However, as it is very difficult to model all possible nonlinear dynamics of a flexible aircraft, solely based on simulations, these models are generally updated using in-flight or wind tunnel test data [5].

Therefore, an Active Aeroelastic Test Bench was designed and built, making the study of low subsonic unsteady aerodynamics and aeroelastic behaviour possible. The experimental data will be used for the validation and development of system identification techniques [6–8] from measured (noisy) data. Some of these methods have already been applied to aeroelastic problems before [9–11].

Wind tunnel aeroelastic experiments with pitch and plunge degrees of freedom have been performed extensively during the last two decades [12–20]. However, most of these experiments use springs combined with a mechanism to create (non-)linear structural behaviour of the wing or aircraft model being tested. These require long set-up time, and it is not easy to change the structural behaviour, because the complete mechanism has to be changed. Next, external excitation of the wing under test is not always possible with those mechanisms.

An aeroelastic test set-up allowing large excitation to be applied to a wing was presented by Babbar et al. in [21–23]. This set-up makes the study of forced-motion unsteady aerodynamic, and aeroelastic experiments possible. On the

one side, the unsteady aerodynamic forces can be measured if the wing is mounted rigidly. On the other side, if the wing is elastically mounted, the aeroelastic response can be measured. However, the main drawback of the proposed set-up is that it can only excite the wing in a harmonic manner at a constant frequency or during a sine-sweep, whereas, the AATB presented here can excite the test model through random excitation.

Another important asset of the AATB is the fact that the real-time controller can be programmed such that the linear actuators behave as (non-)linear springs. This software controllable behaviour makes it very easy to change the structural properties. This can be done even while the set-up is operating.

Diana et. al. [24–26] used a forced motion test bench for unsteady aerodynamic analysis of a bridge deck. That set-up is only capable of forcing the motion of the bridge deck, and the aeroelastic response has to be measured on a different set-up. Therefore, the main advantage of the AATB presented in this paper, is that it is capable of dealing both with forced-motion, as well as aeroelastic experiments in one set-up. This allows to perform many different experiments within a very short time. Therefore the influence of many parameters, such as stiffness and pitch axis location, can be changed.

2 The active aeroelastic test bench

The Active Aeroelastic Test Bench (AATB) is illustrated by the CAD model, as well as a photograph in Figure 1. The complete AATB is mounted in the wind tunnel section, and provides support and actuation for a model in two degrees of freedom (pitch and plunge).

The linear motors actuating the pitch beam, the load cells, and the supporting linear motion mechanism are illustrated. The linear motion mechanism is required to support the model in the 4 remaining degrees of freedom, such that no sideways, fore-aft, roll, and yaw motion of the wing can occur.

Simultaneous movement of the two actuators (Figure 1) results in plunge movement of the supported structure. When a different signal is applied to the actuators a rotation of the pitch beam (Figure 1) occurs.

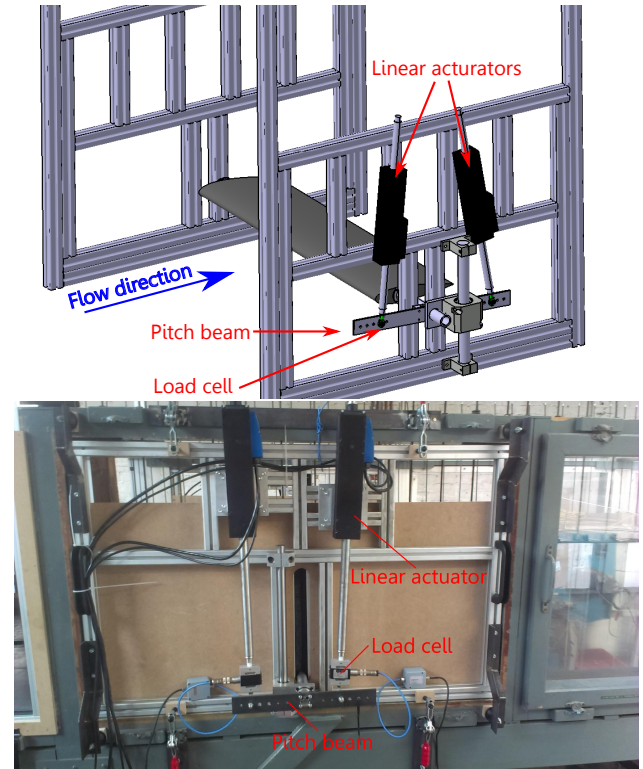


Fig. 1 : The Active Aeroelastic Test Bench.

The general actuation schematic for the Active Aeroelastic Test Bench in both open or closed-loop operation is given in Figure 2. The a real-time processor (dSpace DS-1103) is used to process the recorded forces from the load cells, as well as the position of the wing. The position is obtained from the encoders, mounted on the linear motors. The real-time processor sets, depending on the simulated structural model in closed-loop operation, the position of the wing. In open-loop operation, the real-time processor is used to set the desired position commands to the actuator's control drives.

The actual position of the wind tunnel test model is obtained from the glass scale encoders embedded in the linear actuators. The digital position accuracy of the encoders is 0.0125 mm. Therefore the vertical (heave or plunge) position of the set-up is controlled within this accuracy. Due to

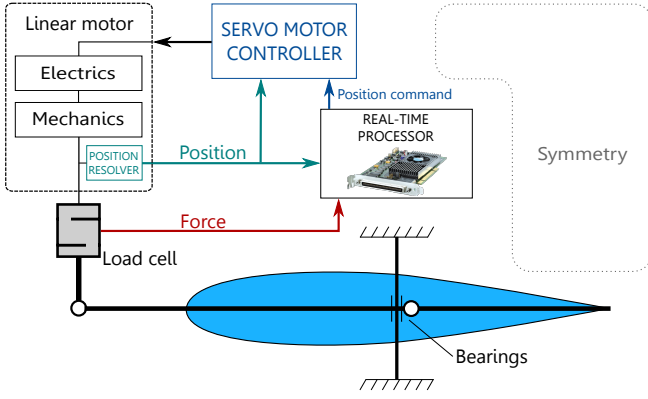


Fig. 2 : Real-time processor board commanding the leading edge actuator of the AATB with feedback from the load sensors, illustrating the different subsystems. The trailing edge actuator system is omitted from the illustration due to symmetry of the system.

the spacing between the front and rear actuators of about 250 mm, an angular resolution of around 0.01 deg is obtained. To set the pitch angle we use Eq. 1, based on the sine of the pitch angle. This relation is illustrated in Figure 3. The distance between the two linear actuators is l , the vertical displacement of the linear actuators are respectively ΔX_1 and ΔX_2 , while θ is the pitch angle.

$$\theta = \sinh\left(\frac{\Delta X_1 + \Delta X_2}{l}\right) \quad (1)$$

Fig. 3 : Simplified calculation of the pitch angle from the displacement of the linear actuators.

Further mechanical properties of the AATB are summarised in Table 1. It is important to notice that due to the inertia of the system, as well as the aerodynamic loads, the maximum pitch and plunge frequency are limited by the required amplitude.

Table 1: Mechanical properties of the Active Aeroelastic Test Bench.

Pitch frequency range	0 - 25 Hz
Plunge frequency range	0 - 25 Hz
Pitch-plunge phase	Arbitrarily variable
Pitch amplitude	± 25 deg
Plunge amplitude	± 15 cm
Maximum plunge force	3000 N (peak 1 s)
Maximum pitch moment	1200 Nm (peak 1 s)

2.1 Open-loop operation of the Active Aeroelastic Test Bench during forced motion experiments

Figure 4 illustrates how position commands are transferred into measured loads after passing through the unsteady aerodynamic system. It is important to realise that the actual input signal to the aerodynamic system in terms of motion of the wing, will be altered by the dynamics of the actuators and their control loop. Therefore, it will not be equal to the commanded position input to the actuators. However, as the actual position of the wing is measured by the encoders of the linear motors, the commanded position signal can be chosen such that the desired input to the unsteady aerodynamic system is obtained.

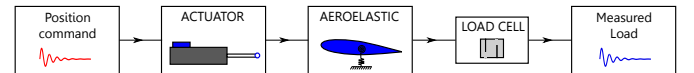


Fig. 4 : The transition from commanded position to recorded load during open-loop operation of the AATB.

In general multisine excitation signals are used as they offer numerous advantages over traditional impulse and sweep signals. In [27], [28], and [29] the advantages of multisine excitation signals for respectively system identification and modal analysis were discussed. The use of multisine signals for the detection of nonlinearities was proposed by [30], whereas the application and advantages of multisine excitation for ground vibration testing and in-flight flutter analysis was discussed in [31].

2.2 The Active Aeroelastic Test Bench in closed-loop operation

The second possible use of the AATB is in closed-loop operation. Figure 5 shows the closed loop operation principle. In contrast to the open loop operation illustrated in Figure 4, the force measurements obtained from the load cells are not only acquired for analysis, but are also fed into the real-time processor. In this real-time processor the raw force signal is filtered and the required displacement of the wing is forwarded to the linear actuators. This forwarded displacement is chosen such to suit the emulated stiffness and damping properties of the structural part within the aeroelastic system.

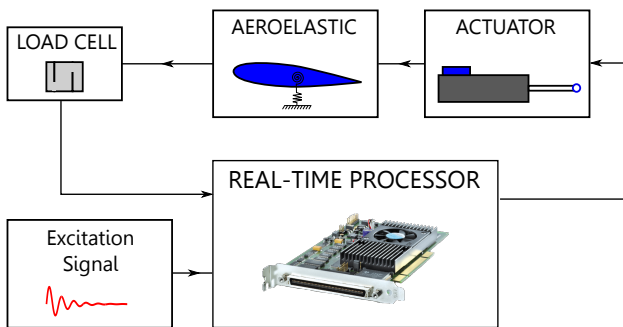


Fig. 5 : The real time processor board commanding the actuators of the AATB with feedback from the load sensors in closed-loop operation.

As aerodynamic loads will vary depending on the excitation signal and the wind velocity, the response of the wing to the applied force by the actuator will also vary. This is dealt with while generating the desired position commands in the structural model emulator by the real-time processor.

Figure 6 shows the servo control loop that is integrated in the AC servo motor control drives. The servo control loop has the purpose of minimizing the error between the desired, and the actual motor position, and this by setting the motor current. The current indirectly sets on its turn the force working on the actuators piston. It is therefore important to tune the servo drives accurately in order to minimize the overshoot, constrained with the fact that the system has to remain stable.

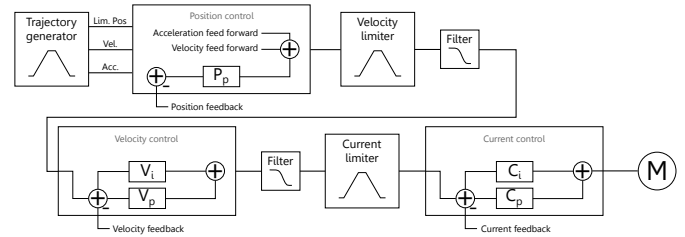


Fig. 6 : Three nested control loops transform the generated motion command from the real-time processor to motion of the linear motor.

3 The experimental set-up for initial testing

A styrofoam wing with constant chord of 350 mm, and NACA 0018 airfoil was mounted in the AATB. Styrofoam was chosen as material as it results in a flexible wing. This is not what one would eventually want when performing forced motion experiments, as deformation of the wing will influence the results from the desired rigid body motion of the wing. However, this flexibility was desired in the start up phase of the AATB, as small miss alignments between the left and right side of the AATB could occur. With a rigid wing, this would lead to failure of the wing or the AATB. The results presented here illustrate the capabilities of the AATB without the purpose of giving benchmark results yet. The styrofoam wing will be replaced by a very stiff composite wing equipped with pressure taps for future measurements.



Fig. 7 : The styrofoam NACA 0018 wing mounted in the AATB.

Therefore, the results presented here shall be used with care, as they do not represent the typical behaviour of a NACA 0018 airfoil, but represent the result obtained with the particular

(elastic) wing being tested. A photograph of the NACA 0018 wing, mounted in the AATB, at lowest possible plunge position, is given in Figure 7. It shall be mentioned that due to the manufacturing of the wing by hot wire cutting of the foam, a relatively rough surface was obtained, which very likely influences the obtained results.

The length of the wing is 1200 mm, which is slightly less than the wind tunnel width of 1280 mm. The height of the wind tunnel used for these initial tests is only 440 mm. This resulted in significant blocking of the airflow at angles of attack above 16° . This issue will be dealt with by moving the AATB to a larger wind tunnel section, and/or, by using a wing with a smaller chord.

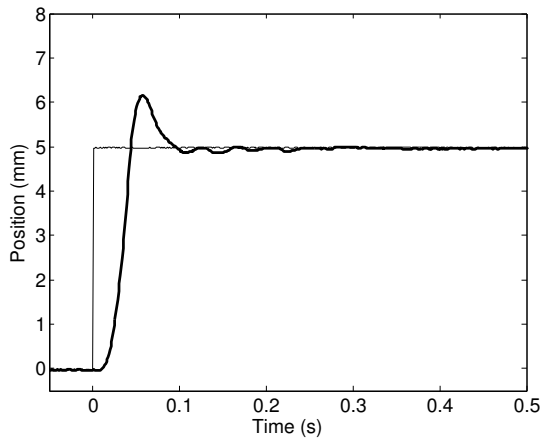


Fig. 8 : Step response of the AATB illustrating 23 % of overshoot, and a settling time of 0.23 seconds.

Figure 8 illustrates the step response for a 5 mm plunge command at 30 m/s. The 2 % settling time of the actuators is 0.23 seconds, and an overshoot of 23 % is observed. A conservative tuning of the servo drives was chosen for initial testing, resulting in a delay and overshoot of the linear motors to the step command.

4 Static analysis of a NACA 0018 airfoil

Figure 9 shows the measured lift coefficient and pitch moment coefficient, obtained with the AATB. For each angle of attack 30 seconds of data was captured, and the averaged values are shown. The Reynolds number is $5.87 \cdot 10^5$, as the

free stream flow velocity was 25 m/s. The maximum lift coefficient ($C_{L,max}$), the lift curve slope $C_{L,\alpha}$ and the zero angle of attack lift and pitch moment coefficient ($C_{L,0}, C_{m,0}$) are given in Table 2. The pitch moment C_m is given at the quarter chord point.

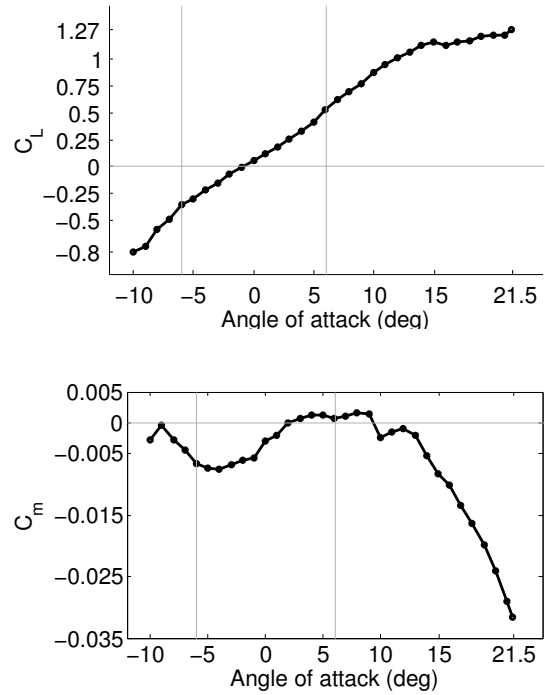


Fig. 9 : Measured lift- and pitch moment coefficient as a function of the angle of attack for a NACA 0018 at 25 m/s.

Table 2: Identified aerodynamic coefficients for a NACA 0018 at Reynolds number of 5.87×10^3 .

$C_{L,max}$	1.27
$C_{L,\alpha}$	4.27
$C_{L,0}$	0.061
Linear range	± 6 deg
$C_{m,0}$	-0.003

5 Response at small pitch angle

5.1 The 1 Hz forced motion

Figure 10 shows the pitch angle measured at a 1 Hz sine excitation as a function of time in the upper part, and the following error between the commanded and the pitch angle, in the lower part.

The Reynolds number for this experiment was $7 \cdot 10^5$, as the velocity was set at 30 m/s. Therefore, the reduced frequency $k = \frac{\omega \cdot c}{2V}$ was equal to 0.0367. With ω the forcing frequency, c the chord in meters, and V the free stream air velocity. Notice that we use pitch angle here in stead of angle of attack, as for a moving airfoil these are not any more equal. An induced angle of attack is introduced due to the motion of the wing, resulting in an effective angle of attack, depending both on the pitch angle and the pitch velocity [32].

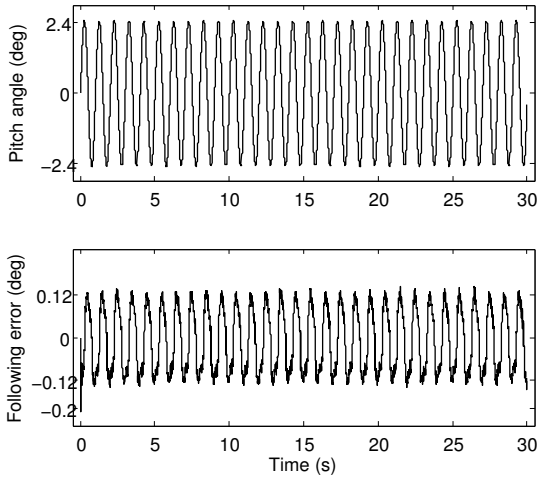


Fig. 10 : Measured pitch angle and following error for a 1 Hz sine in the linear range.

From the bottom part of Figure 10 one can see that the following error reaches values up to 0.12 deg for a commanded pitch angle of 2.4 deg, which is an error of 5 %. It shall, however, be noticed that this following error is perfectly harmonic, with the same frequency as the measured (and commanded) pitch angle. This results in the amplitude spectra of the commanded (cyan) and the measured pitch angle (black) in Figure 11 to be equal for the excitation frequency of 1 Hz. From analysing the time domain data it was found that the measured pitch angle lags 8 ms behind the commanded pitch angle. Therefore, we conclude that the control loop of the actuators, being based on correcting the error between the desired and obtained position, introduces a delay between the commanded and desired value. However, as we measure the actual position of the actuators, this is not a problem in analysing

the relation between the forced displacement and the occurring loads.

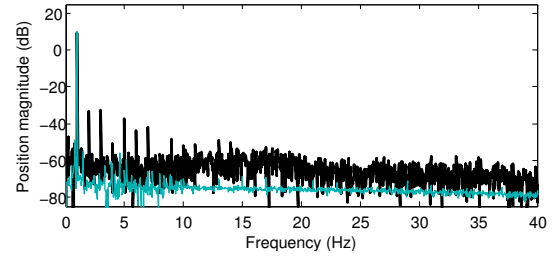


Fig. 11 : Spectrum of the measured and commanded pitch angle for a 1 Hz sine in the linear range.

Except for the peak at 1 Hz, which is the forcing frequency, some smaller peaks are noticed at integer multiples of this 1 Hz forcing frequency. These are nonlinear distortions that appear in the measured spectra. Although, they are very distinct in the spectrum shown in Figure 11, there is almost no distortions visible in the time domain signal of Figure 10. This, because the amplitude of the nonlinear distortions on the actuator is 40 dB lower than the amplitude measured at the forcing frequency, and is thus 100 times smaller. The non-linear distortions visible in the spectrum of the position of Figure 11 can therefore be neglected for the position readouts. The reason why they are so clearly visible is due to the very low noise level on the position measurements, which yields a very high signal-to-noise ratio of 70 dB.

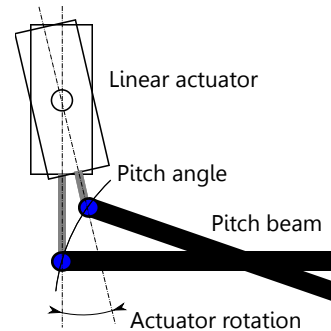


Fig. 12 : Actuator motion results in a nonlinear relation between commanded and obtained pitch motion.

The occurrence of these nonlinear harmonics are thought to be caused by the kinematics of the

AATB. The small angle assumption is used to relate pitch angle to displacements of the linear motors. This assumption, however, does not take into account that the actuator will rotate in order to compensate the horizontal displacement, due to the rotating motion of the pitch beam. Therefore, an actuator displacement of 5 mm will not result in a 5 mm vertical displacement of the pitch beam, but a slightly smaller value. This is illustrated in Figure 12. Thus, the sine requested for the pitch angle is not a perfect sine, but is slightly disturbed. As the angle of attack and pitch angle are reconstructed from the position readout of the linear motors, the actual magnitude of these nonlinearities in the pitch angle are larger, but unknown. Although, as the geometry of the AATB is exactly known, one can compensate for these nonlinear distortions to the pitch angle. However, this was not yet completed in this work.

5.2 Lift response to the 1 Hz sine

Next, we will discuss the measured lift forces as a response to this 1 Hz forced motion. As we previously mentioned, the applied sine will contain some nonlinear distortions due to the kinematics of the AATB. Therefore we expect to find these higher harmonics back in the measured lift force spectra.

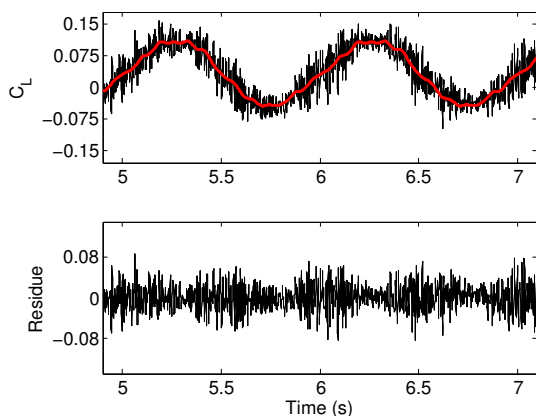


Fig. 13 : Smoothed and raw lift coefficient response for a 1 Hz forced sine of $\pm 2.4^\circ$.

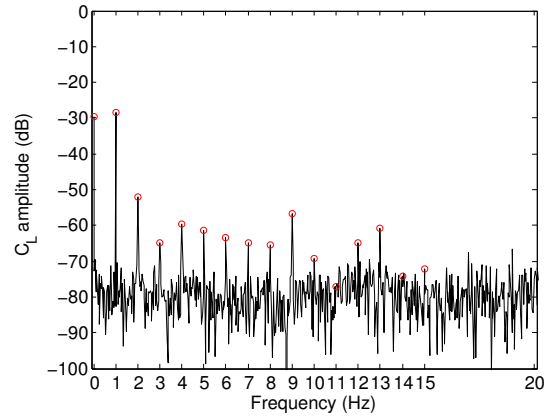


Fig. 14 : Small nonlinear contributions in the lift coefficient spectrum at higher harmonics for a 1 Hz forced sine of $\pm 2.4^\circ$.

The lift force generated by the 1 Hz sine motion of the wing is illustrated both in the time domain, as well as in the frequency domain, in respectively Figures 13 and 14. For the time domain plot, both the smoothed and raw data are plotted in the top part of the figure. In the bottom part, the residue between the smoothed and raw data is shown. The smooth signals were constructed by taking the inverse fast Fourier transform from the selected lines, indicated with a dot, in Figure 15.

As the position spectrum contained nonlinear contributions at higher harmonics than the 1 Hz forcing frequency, also the load response spectrum contains these higher harmonics as seen in Figure 14. The attenuation has a difference of more than -20 for the amplitude, therefore the nonlinear harmonics in the force spectrum are 10 times smaller than the response at the 1 Hz forcing frequency. However, their influence is not negligible, because there are 14 higher harmonics with some energy contents. If one sums all of these, the total contribution of the higher harmonics is still significant compared to the response for the 1 Hz forcing frequency.

The influence of including the higher harmonics in the lift coefficient C_L as a function of the pitch angle, is illustrated in Figure 15. In which the grey bullets show the measured values, and the lines the smoothed relation. The brighter the line, the more higher harmonics are included. The black line includes no higher harmonics, and il-

illustrates the response at 1 Hz. An elliptical pattern is recognised. This comes from the dynamic relation between the pitch angle and lift coefficient, as the pitch velocity has a significant contribution to the generated lift force. The pitch velocity is opposite if the wing pitches up or down, declaring this ellipse, rather than a straight line. The bright orange line includes all 15 higher harmonics.

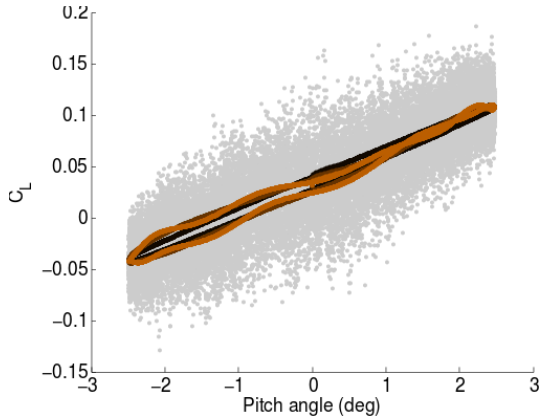


Fig. 15 : Including the nonlinear higher harmonics for the lift coefficient as a response to a 1 Hz forced sine of $\pm 2.4^\circ$ yields no significant changes to the lift coefficient in function of the pitch angle.

It can be concluded that even if no higher harmonics are included, we still find a small difference between the up- and down pitching trajectory. Theodorsen [32] discussed this behaviour, which is caused by the motion of the wing, introducing an effective angle of attack. This behaviour was also observed during the pitch oscillation experiments described in [22]. Further study at different reduced frequencies k will be performed to quantify these effects, and compare with theoretical models from [32] and [33].

We conclude from these small pitch angle experiments that it will be required to study further the kinematics of the AATB in order to be able to quantify their influence to the measured force response. This in order to allow the further study of the influence of the reduced frequency k on the effective lift coefficient at a given pitch angle and velocity.

6 Small oscillations around a large pitch angle

After analysing the resulting lift force for an oscillation at a small angle of attack, well within the linear range of the measured lift curve from Figure 9, an experiment at high pitch angle was performed. The wing was forced to pitch 2.4° at a frequency of 1 Hz, around an 18.5° set point. The wind velocity was set at 20 m/s. Therefore the Reynolds number was 4.7×10^5 , and the reduced frequency $k = \frac{\omega \cdot c}{2V} = 0.055$.

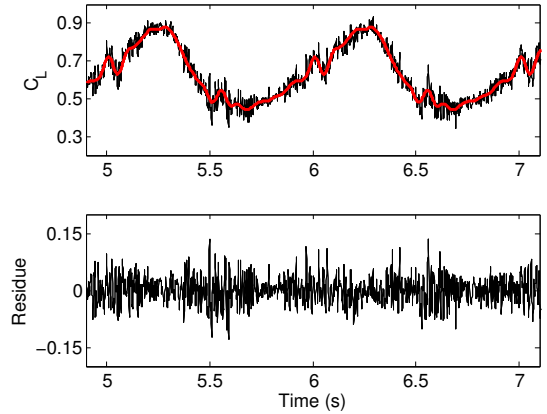


Fig. 16 : Two periods of the raw and smoothed lift coefficient (top), and the residue (bottom), for the large pitch angle experiment.

The resulting lift coefficient, after subtracting the inertial loads from the total measured loads, is shown in Figure 16. Both the resulting lift coefficient measurements, and the smoothed values are illustrated for two periods of the 1 Hz forcing frequency. The smoothed lift coefficient values are obtained from selecting the 1 Hz response, and the 14 higher harmonics in the spectrum of the identified instantaneous lift coefficient, given in Figure 17. This procedure is the same as the one used for the small pitch angle experiments.

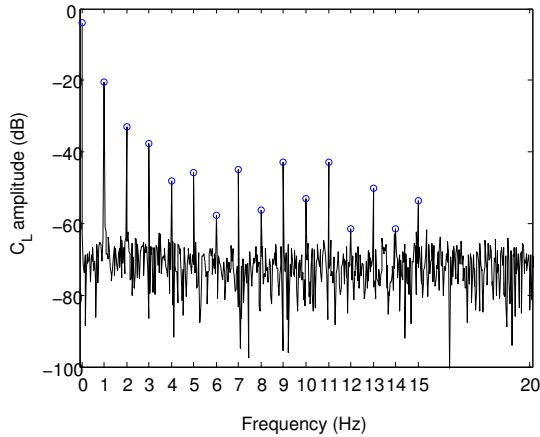


Fig. 17 : Significant harmonics occur in the spectrum of the lift coefficient in the nonlinear range about a large pitch angle.

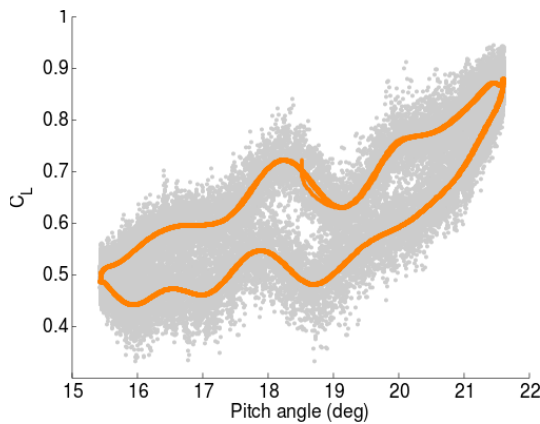


Fig. 18 : Instantaneous relation between the lift coefficient and the angle of attack when all the harmonics responses are included from the large pitch angle experiment.

From the lift coefficient spectrum we can notice that, except for the DC component which is the 18.5° set point angle, and the 1 Hz forcing excitation, a lot of high amplitude harmonics exist at integer multiples of this 1 Hz forcing frequency. These harmonics are a result from the nonlinear pitch angle due to the kinematics of the AATB, and the nonlinear aerodynamic response at high angle of attack.

When all the harmonics are included to obtain the smoothed values of the lift coefficient, as used in Figure 16, the relation between lift coefficient and instantaneous pitch angle is illustrated in Fig-

ure 18. The smoothed values are shown on top of the actual measured values.

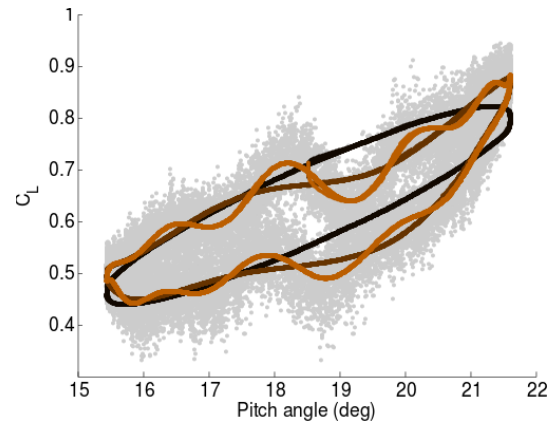


Fig. 19 : The evolution when included more harmonics to the smoothed data for the lift coefficient from the experiment at large pitch angle.

The instantaneous relation between the assumed pitch angle, and the lift coefficient C_L , for the higher amplitude pitch oscillation experiments is illustrated in Figure 18. As mentioned before, an error is introduced by assuming that a linear relation exists between the pitch angle and the displacement of the linear actuators.

The difference between including these higher harmonics due to the nonlinear response is even greater than for the small angle experiment. Figure 19 illustrates the influence of including none, half, or all of the higher harmonics. The larger differences are as expected due to the larger pitch angle. Which increases the error from assuming a linear relation between the pitch angle and the actuator displacement. Additionally, nonlinear aerodynamics occur at these higher angles of attack. Therefore, it is impossible, without including the nonlinear kinematics of the AATB, to distinguish whether the nonlinear forces are occurring due to nonlinear kinematics of the wing, or aerodynamic phenomena.

7 Conclusions and further work

In this paper a new test set up for the study of unsteady aerodynamics and aeroelastic experiments

was introduced. We can conclude from the preliminary results, that the set-up is capable of applying a forced motion with frequencies up to 25 Hz in both pitch and plunge degrees of freedom. During these forced motion experiments, the phase between the pitching and plunging motion can be set arbitrarily. Additionally, also the chordwise location of the pitch axis can be set by the user.

The preliminary results show that it is necessary to include the detailed kinematics of the AATB in the preprocessing of the measured data, to correctly identify the relation between pitch angle and lift coefficient. Even for very small amplitude oscillations of $\pm 2.4^\circ$ a significant error is introduced by assuming a linear relation between the linear actuators positions and the pitch angle. The higher harmonics present in the spectra of the lift coefficient for both the small amplitude oscillations, and even more for the large amplitude oscillations, illustrate that the nonlinear kinematics can not be neglected.

The preliminary tests reported in this paper have located the weaknesses of the AATB, being: the tuning of the servo motor drives, and the nonlinear kinematics of the AATB. These, however, are well known engineering topics, which are very likely to be solved easily. As the relation between the pitch angle and the occurring forces will then be exactly known, the influence of pitch axis location, pitch velocity and reduced frequency, will then be studied.

Additionally, the AATB will be further extended with load cells to also measure the drag forces. Next to the direct force measurements, the test wing will also be equipped with up to 64 pressure taps, allowing to study the pressure distribution around the airfoil during the forced motion experiments.

Acknowledgements

This work is sponsored by the Research Council of the Vrije Universiteit Brussel, the Strategic Research Project OptiMECH, the Research Foundation Flanders (FWO-Vlaanderen),

the Flemish Government (Methusalem Fund METH1), and the Belgian Federal Government (Interuniversity Attraction Poles programme IAP VII DYSCO).

References

- [1] G. Looye. Integrated Flight Mechanics and Aeroelastic Aircraft Modeling using Object-Oriented Modeling Techniques. In *Modeling and Simulation Technologies Conference and Exhibit*, pages 1–11, 1999.
- [2] R. Cook, R. Palacios, P. Goulart, and I. Roberts. Robust manoeuvring and gust alleviation of very flexible aircraft using novel control effectors. In *IFASD 2011 - 15th International Forum on Aeroelasticity and Structural Dynamics*, pages 1–34, Paris, France, June 2011.
- [3] A. Wildschek, F. Stroscher, T. Klimmek, Z. Šika, T. Vampola, M. Valášek, D. Gangsaas, N. Aversa, and A. Berard. Gust load alleviation on a large blended wing body airliner. In *27th Congress of the International Council of the Aeronautical Sciences*, Nice, France, September 19 – 26, 2010.
- [4] J. Murua, R. Palacios, and J. M. R. Graham. Open-Loop Stability and Closed-Loop Gust Alleviation on Flexible Aircraft Including Wake Modeling. In *53rd AIAA/ASME/ASCE/AHS/ASC Structures, Structural Dynamics and Materials Conference*, number April, pages 1–23, Honolulu, Hawaii., April 23 – 26, 2012.
- [5] R. Lind and M. Brenner. Incorporating Flight Data into a Robust Aeroelastic Model. *Journal of Aircraft*, 35(3):470 – 478, 1998.
- [6] R. Pintelon, P. Guillaume, Y. Rolain, Joannes Schoukens, and H. Van Hamme. Parametric identification of transfer functions in the frequency domain—a survey. *IEEE Transactions on Automatic Control*, 39(11):2245–2260, 1994.
- [7] J. Schoukens, R. Pintelon, T. Dobrowiecki, and Y. Rolain. Identification of linear systems with nonlinear distortions. *Automatica*, 41(3):491–504, March 2005.

- [8] J. Lataire, R. Pintelon, and E. Louarroudi. Non-parametric estimate of the system function of a time-varying system. *Automatica*, 48(4):666–672, Apr. 2012.
- [9] J. Ertveldt, J. Lataire, R. Pintelon, and S. Vanlanduit. Frequency-domain identification of time-varying systems for analysis and prediction of aeroelastic flutter. *Mechanical Systems and Signal Processing*, 47(1–2):225–242, August 2014.
- [10] P. Verboven, B. Cauberghe, P. Guillaume, S. Vanlanduit, and E. Parloo. Modal parameter estimation and monitoring for on-line flight flutter analysis. *Mechanical Systems and Signal Processing*, 18(3):587–610, May 2004.
- [11] T. De Troyer, P. Guillaume, C. Devriendt, and M. Runacres. Combined use of FRFs and transmissibility functions in an OMAXframework. In *Proceedings of ISMA2010–International Conference on Noise and Vibration Engineering including USD2010*, pages 3263–3273, Leuven, Belgium, September 2010.
- [12] J. Rivera, B. Dansberry, M. Farmed, C. Eckstrom, D. Seidel, and R. Benett. Experimental flutter boundaries with unsteady pressure distributions for the NACA 0012 benchmark model. In *32nd Structures, Structural Dynamics, and Materials Conference*. American Institute of Aeronautics and Astronautics, 1991.
- [13] B. E. Dansberry, M. H. Durham, R. M. Bennett, J. A. Rivera, W. A. Silva, C. D. Wieseman, and D. L. Turnock. Experimental unsteady pressures at flutter on the supercritical wing benchmark model. In *34th Structures, structural dynamics and materials conference*, April 1993.
- [14] G. Dietz, G. Schewe, and H. Mai. Experiments on heave/pitch limit-cycle oscillations of a supercritical airfoil close to the transonic dip. *Journal of Fluids and Structures*, 19(1):1–16, January 2004.
- [15] T. Lee and P. Gerontakos. Investigation of flow over an oscillating airfoil. *Journal of Fluid Mechanics*, 512:313–341, 2004.
- [16] H. Mai, J. Neumann, and H. Hennings. Gust Response: A Validation Experiment and Preliminary Numerical Simulations. In *IFASD 2011 - 15th International Forum on Aeroelasticity and Structural Dynamics*, pages 1–20, Paris, France., June 27 – 30 2011.
- [17] J. Song, T. Kim, and S. J. Song. Experimental determination of unsteady aerodynamic coefficients and flutter behavior of a rigid wing. *Journal of Fluids and Structures*, 29:50–61, February 2012.
- [18] N. A. Razak and G Dimitriadis. Aeroelastic response of a 2-DOF wing with structural and aerodynamic nonlinearity. In *IFASD 2013 – 16th International Forum on Aeroelasticity and Structural Dynamics*, pages 1–13, Bristol, United Kingdom, June 24–27 2013.
- [19] T. Andrianne, B. Korbahti, and G. Dimitriadis. Wind tunnel analysis of separated aerodynamics leading to different types of torsional flutter in bluff-bodies. In *IFASD 2011 - 15th International Forum on Aeroelasticity and Structural Dynamics*, pages 1–20, Paris, France, June 2011.
- [20] N. Muturi, A. Spies, K. Bender, and Christopher L. Lee. Stall Flutter Oscillation Measurements from a Two-Degree-of-Freedom Airfoil with Nonlinear Stiffness. In *54th AIAA/ASME/ASCE/AHS/ASC Structures, Structural Dynamics, and Materials Conference*, pages 1–8, Boston, Massachusetts, April 8-11 2013.
- [21] Y. Babbar and V. S. Suryakumar. An Approach for Prescribed Experiments for Aerodynamic - Structural Dynamic Interaction. In *51st AIAA Aerospace Science Meeting Including the New Horizons Forum and Aerospace Exposition*, number January, Grapevine (Dallas/Ft. Worth Region), Texas, 07 – 10 January 2013.
- [22] Y. Babbar, V. S. Suryakumar, and T. W. Strganac. Experiments in Free and Forced Aeroelastic Response. In *51st AIAA Aerospace Science Meeting Including the New Horizons Forum and Aerospace Exposition*, number January, Grapevine (Dallas Ft. Worth Region), Texas, 07 – 10 January 2013.
- [23] Y. Babbar, V. S. Suryakumar, and T. W Strganac. Experiments in Aeroelastic Response and Control under Gust. In *54th AIAA/ASCE/AHS/ASC Structures, Structural Dynamics, and Materials Conference*, pages 1–10, Boston, Massachusetts, 8 – 11 April 2013.

- [24] G. Diana, F. Resta, A. Zasso, M. Belloli, and D. Rocchi. Forced motion and free motion aeroelastic tests on a new concept dynamometric section model of the messina suspension bridge. *Journal of Wind Engineering and Industrial Aerodynamics*, 92(6):441–462, May 2004.
- [25] G. Diana, D. Rocchi, T. Argentini, and S. Muggiasca. Aerodynamic instability of a bridge deck section model: Linear and nonlinear approach to force modeling. *Journal of Wind Engineering and Industrial Aerodynamics*, 98(6–7):363–374, June 2010.
- [26] G. Diana, D. Rocchi, and T. Argentini. An experimental validation of a band superposition model of the aerodynamic forces acting on multi-box deck sections. *Journal of Wind Engineering and Industrial Aerodynamics*, 113:40–58, February 2013.
- [27] J. Schoukens, P. Guillaume, and R. Pintelon. Design of multisine excitations. In *Control 1991. Control'91., International Conference on*, pages 638–643. IET, 1991.
- [28] P. Guillaume, P. Verboven, S. Vanlanduit, and E. Parloo. Multisine excitations- new developments and applications in modal analysis. In *IMAC-XIX: A Conference on Structural Dynamics*, volume 2, pages 1543–1549, Hyatt Orlando, Kissimmee, Florida, 2001.
- [29] R. Pintelon and J. Schoukens. *System Identification: A Frequency Domain Approach*. John Wiley & Sons, April 2012.
- [30] K. Vanhoenacker, T. Dobrowiecki, and J. Schoukens. Design of multisine excitations to characterize the nonlinear distortions during FRF-measurements. *Instrumentation and Measurement, IEEE Transactions on*, 50(5):1097–1102, 2001.
- [31] T. De Troyer, P. Guillaume, and M. C. Runacres. New excitation and measurement techniques to integrate GVT and flight flutter testing. In *IFASD 2013 - 16th International Forum on Aeroelasticity and Structural Dynamics*, Bristol, United Kingdom., June 2013 2013.
- [32] T. Theodorsen. General theory of aerodynamic instability and the mechanism of flutter. *NACA Technical Report 496*, NASA, Langley Research Center, Hampton, VA, USA., page 26, 1934.
- [33] S. Brunton and C. Rowley. Modeling the unsteady aerodynamic forces on small-scale wings. In *47th AIAA Aerospace Sciences Meeting including The New Horizons Forum and Aerospace Exposition*, Orlando, Florida, January 2009. American Institute of Aeronautics and Astronautics.

Copyright Statement

The authors confirm that they, and/or their company or organization, hold copyright on all of the original material included in this paper. The authors also confirm that they have obtained permission, from the copyright holder of any third party material included in this paper, to publish it as part of their paper. The authors confirm that they give permission, or have obtained permission from the copyright holder of this paper, for the publication and distribution of this paper as part of the ICAS 2014 proceedings or as individual off-prints from the proceedings.